"Single-cycle" ionization effects in laser-matter interaction

Enrique Conejero Jarque* and Fulvio Cornolti†

Dipartimento di Fisica, Universitá di Pisa, Piazza Torricelli 2, Pisa, Italy

Andrea Macchi† and Hartmut Ruhl‡

Theoretical Quantum Electronics, Darmstadt University of Technology, Darmstadt, Germany

Abstract

We investigate numerically effects related to "single-cycle" ionization of dense matter by an ultra-short laser pulse. The strongly non-adiabatic response of electrons leads to generation of a MG steady magnetic field in laser-solid interaction. By using two-beam interference, it is possible to create periodic density structures able to trap light and to generate relativistic ionization fronts.

I. INTRODUCTION

In the adiabatic field ionization regime, the ionization rate grows sharply when the electric field approaches the barrier suppression (BS) limit, i.e. when the laser intensity is high enough that the electron in the ground state is able to "classically" escape the atomic potential barrier. The ionization rate for such field strength may become higher than the

*On leave from Departamento de Física Aplicada, Universidad de Salamanca, Spain. E-mail address enrikecj@gugu.usal.es

†Also INFM, sezione A, Universitá di Pisa, Italy

‡Present address Max-Born Institut, Max-Born str. 2a, 12489 Berlin, Germany

laser frequency and a regime in which most of the ionization is produced within a single laser half-cycle is achievable.

Here we present a numerical study of some effects of ultrafast ionization in the interaction of a short laser pulse with an initially transparent dense medium. First, we will discuss the generation of megagauss steady magnetic fields in the surface "skin" layer of "solid" targets, i.e. slabs of hydrogen atoms with a number density close to that of a solid medium (Macchi et al. 1999).

Second, we will describe effects related to the combination of two-beam interference with ultrafast ionization. We will show how it is possible to take advantage of this feature to create a layered dielectric-conductor structure able to trap the electric field, as well as a relativistic ionization front (Conejero Jarque et al. 1999).

II. GENERATION OF STEADY MAGNETIC FIELDS

The generation of steady currents and magnetic fields by ultrafast ionization is due to the non-adiabatic nature of the response of initially bound electrons to a strongly ramping laser field. Using a following "simple-man's" model (SMM), very similar to the SMM used in studies of above-threshold ionization and harmonic generation in atoms, it can be shown that a single electron subject to an external sinusoidal intense field can acquire a steady velocity (Macchi et al. 1999)

$$v_{st} = v_I - v_{qo}\sqrt{1-(E_T/E_{yo})^2}, \tag{1}$$

where v_I is the ejection velocity of the electron, $v_{qo} = eE_{y0}/m\omega$, E_{yo} is the maximum field amplitude and E_T is the field amplitude at the instant of ionization, which will be close to the threshold field for barrier suppression (for hydrogen, $E_T \approx 0.146 E_{au} = 7.45 \times 10^8$ V cm^{-1}, being $E_{au} = 5.1 \times 10^9$ V cm^{-1} the atomic field unit).

If most of the electrons in the medium are ionized at the same instant, as may happen with a pulse which sharply rises above E_T, one gets a net steady current which in turn

generates a magnetic field. To obtain a larger current one may think to "tune" appropriately E_T and E_{y0}. This is possible if the ionization is no longer correlated with the oscillating field, i.e., it is produced *independently* of the field itself, like in the case studied by Wilks et al. (1988), in which a steady magnetic field $B_{st} \approx E_{y0}$ can be obtained in a very dense medium. For intense lasers ($I \geq 10^{18}$ W cm^{-2}), such a magnetic field would get values exceeding 100 MG and could explain (Teychenné et al. 1998) the experimental observation of high transparency of thin foil solid targets to 30 fs, 3×10^{18} W cm^{-2} pulses (Giulietti et al., 1997). However, it is questionable whether this high magnetic field may be obtained with superintense laser pulses. In this case, in fact, the "source pulse" itself ionizes the medium and thus this will impose a constraint on the phase mismatch between the field and the velocity of the electrons. We will show by numerical simulations that the steady magnetic field exists but has values around 1 MG, being therefore too weak to allow enhanced laser propagation.

A. PIC simulations

First we review the results of 1D3V PIC simulations with field ionization included. We choose pulses with a "sin^2" envelope and with a "square" envelope. For all the PIC runs, the laser frequency was $\omega_L = 2 \times 10^{15}$ s^{-1}, close to that of Nd and Ti:Sapphire lasers. The thickness of the target was $0.09\,\mu$m and the density was $n_o = 6.7 \times 10^{22}$ cm^{-3} ($\omega_{po} \simeq 7\omega_L$). For the ionization rate we used a semi-empirical formula obtained from atomic physics calculations (Bauer and Mulser, 1999). The laser energy loss due to ionization is included introducing a phenomenological "polarization" current (Rae and Burnett 1992, Cornolti et al. 1998, Mulser et al. 1998).

Fig.1 shows the spatial profiles of the magnetic field and the free electron density five cycles after the end of a five cycles long ($\Delta t_L = 15$ fs) pulse, for three different field intensities in the "sin^2" shape case, and for the square profile case at the intermediate intensity value. The steady field is generated at the beginning of the interaction and is always much weaker

than the laser field, even for the most intense case (corresponding to an intensity of 3.5×10^{18}W cm^{-2}); its sign varies according to the phase of the laser half cycle where most of the ionization occurs. The ionization at the left boundary is nearly instantaneous; however, even if the target is only 0.1λ thick, it is not ionized over its whole thickness due to instantaneous screening, except for the maximum intensity case.

The fact that the produced magnetic field is much less than expected may be attributed to the instantaneous screening of the EM wave due to the ultrafast ionization. In fact, it is too weak to affect self-consistently the refractive index and as a consequence it cannot lead to magnetically induced transparency as hypothesized by Teychenné et al. (1998).

B. Boltzmann simulations

To yield a further insight into the magnetic field generated by ultrafast ionization we look at the results of 1D and 2D Boltzmann simulations. This corresponds to the "direct" numerical solution of the Boltzmann equation for the electron distribution function $f_e = f_e(\mathbf{x}, \mathbf{v}, t)$, over a phase space grid:

$$\partial_t f_e + \mathbf{v} \cdot \nabla f_e - \frac{e\mathbf{E}}{m} \cdot \partial_{\mathbf{v}} f_e = \nu_I(E) n_a(\mathbf{x}, t) g(\mathbf{v}; \mathbf{E}(\mathbf{x}, t)). \tag{2}$$

Here n_a is the density of neutral atoms (supposed at rest for simplicity) and ν_I is the ionization rate. The term $g(\mathbf{v}; \mathbf{E})$ gives the "instantaneous" distribution of the just ionized electrons, which is supposed to be known from atomic physics. A semiclassical picture which allows to define and evaluate $g(\mathbf{v}; \mathbf{E})$ was given by Cornolti et al. (1998). With respect to PIC simulations, the Boltzmann approach has the disadvantage of larger memory requirements, but the advantages of reduced numerical noise and the possibility to take into account the full kinetic distribution of the ionized electrons.

We first look at 2D2V Boltzmann simulations. We take a $0.25\,\mu$m, 10^{16} W cm^{-2} laser pulse impinging on a solid hydrogen target with number density 2×10^{23} cm$^{-3} = 12.5 n_c$, and thickness $0.1\,\mu$m. The time envelope of the laser pulse is Gaussian with a FWHM duration

of 2 cycles. The laser spot is also Gaussian with a FWHM of $2\,\mu$m. Fig.2 (a) shows the magnetic field and the density contours after the end of the laser pulse. The steady magnetic field has constant (negative) sign over its extension. Its maximum intensity is about 3 MG. Fig.2 (b) shows the electron current density j_y at the same time of the right plot of fig.2 (a).

Among the parameters of our simulations, the magnetic field appears to be most sensitive to the temporal profile of the laser pulse, achieving its maximum value for a square pulse with zero risetime. In Fig.3 (a) we show the results of a 1D Boltzmann simulations for a square pulse with $I = 10^{16}$W cm^{-2}, $\lambda = 0.25\,\mu$m, and a target with $n_e/n_c = 12.5$. The current density is $j_y \sim 10^{22}$ c.g.s. units and extends over a distance comparable to $d_p \simeq 1.2 \times 10^{-2}\,\mu$m. The maximum magnetic field is consistent with Ampere's law, which gives $B_{st} \sim 4\pi j_y d_p/c \simeq 5$ MG. Assuming a density $n_e \simeq n_o = 2.2 \times 10^{23}$ cm^{-3} for the electrons which are instantaneously ionized, one gets a steady velocity $v_{st} \simeq j_y/en_e \simeq 10^8$ cm s^{-1}. This value is lower than the ejection velocity for hydrogen $v_I \simeq 2\times 10^8$ cm s^{-1}. This suggests that effects such as screening, nonzero ionization time, and velocity statistics act to keep the steady current well below the values that one may estimate according to the SMM, eq.(1).

Both laser and target parameters where varied in simulations in order to investigate the scaling of the magnetic field with them. As an example, Fig.3 (b) shows the results of a simulation for a target of hydrogenic ions with density and thickness identical to Fig.3 (a), but where we assumed a nuclear charge $Z = 2$ and scaled the atomic parameters accordingly to $\mathbf{x} \to Z\mathbf{x}$, $t \to Z^2 t$, $\omega \to Z^{-2}\omega$, $\mathbf{E} \to Z^{-3}\mathbf{E}$. In order to have the ionization threshold to be exceeded at the same instant, the laser pulse had the same envelope and frequency but the intensity was scaled by Z^6. With respect to the $Z = 1$ case, we obtain a steady field with *lower* peak amplitude which assumes both positive and negative values.

We also performed 2D Boltzmann simulations for a pulse obliquely incident at 15^o on the target. The preliminary results show that the magnetic field is much lower in this case. Therefore it appears that the steady magnetic field is sensitive to the interaction geometry. In any case, the oblique incidence results further confirm the conclusion that no magnetic field capable to affect the transmission through the target is generated.

III. OPTICAL MICROCAVITIES AND IONIZATION FRONTS

A. The model

In this section, we study effects related to two beam-interference in one spatial dimension and for wavelengths in the infrared and optical range. In our numerical experiment, a one-dimensional interference pattern is generated via an appropriate "target manufacturing": the idea is to place a reflecting mirror on the rear side of the target, the one opposite to the laser. Such a mirror might be easily produced by a metallic coating on a glass or plastic target. Taking a laser pulse with peak intensity between $I_T/2$ and I_T, being I_T the "threshold" value for ionization, a plasma is produced in the target bulk around the maxima of interference pattern produced by the incident wave and the wave reflected at the rear mirror.

Since in this regime we deal only with moderate laser intensities, we may use a simple one-dimensional fluid model based on continuity, current and wave equations for an ionizing medium, originally proposed by Brunel (1990), modified by the inclusion of the polarization current. More details about the model and its validity can be found in Cornolti et al. (1998) and Conejero Jarque et al. (1999).

B. Generation of layered plasmas

We first consider a target with thickness $L = 2\pi\lambda$, being $\lambda = 0.8\,\mu$m, and density $n_o = 10n_c$. The laser pulse has a $\sin^2$-shaped envelope with a duration of 80 fs (30 cycles) and a peak intensity $I = 1.8 \times 10^{14}$ W cm^{-2}. The target parameters are chosen to simulate a thin foil solid slab and it is enough to take the density as low as $10n_c$ since the maximum electron density always remains much lower than this value.

The electron density vs. space and time is shown in Fig.4. A clear layered density pattern with a spatial periodicity close to $\lambda/2$ is produced along nearly all the slab. The layers of overdense plasma are produced near the maxima of the interference pattern. These maxima

appear at close times because of the effect of the smooth envelope of the laser pulse. The resulting quasi-periodic structure of the refractive index has in principle some similarities with the widely studied semiconductor microcavities and photonic band-gap materials (see reviews by Burstein and Weisbuch (1993) and by Skolnick et al. (1998)).

C. Optical microcavities

Since the density in the plasma layers is overcritical, and the layers are created in a time shorter than a laser halfcycle, the portions of the standing wave between adjacent intensity maxima may be "trapped" into the cavity formed by the two neighboring layers. This trapping effect is best seen in the case of a CO_2 pulse impinging over a gas target with $L = \lambda = 10.6\,\mu$m and $n_o = 5n_c \simeq 5 \times 10^{19}\text{cm}^{-3}$. For this target, two plasma layers are produced around the positions $x = 0.25\lambda, x = 0.75\lambda$. Fig. 5 shows the map of the electric field at early (a) and later (b) times, showing the generation of the constructive interference pattern which yields the layered ionization (a), and the subsequent trapping of the field which remains in the cavity at times longer than the incident pulse duration (b). The non-ionized regions between density layers clearly act as optical microcavities.

Since the microcavity length is $L_c \leq \lambda/2$, light must have an upshifted wavevector $k' \geq k$ in order to persist inside the cavity. This implies also upshift of the laser frequency with $\omega'_L \geq \omega_L$ as seen in Fig.5(b). The upshift decreases the critical density value for the trapped radiation and therefore wavelengths much shorter than λ escape from the cavity. Due to the small fraction of light that tunnels out of the cavity one observes radiation emission from the target for a time much longer than the pulse duration. Both the frequency upshift and the pulse lengthening may provide experimental diagnostics for microcavity generation. The lifetime of the cavities is ultimately limited by processes such as recombination, which however should appear on times much longer than the pulse duration of a few tens of femtoseconds that are considered here and are available in the laboratory.

D. Ionization fronts

As already shown, in our model target ionization is produced around the maxima of the "standing" wave which is generated due to the reflection at the rear mirror. However, since ionization is instantaneous on the laser period timescale, it is produced as soon as the wave reflected at the rear mirror travels backwards and builds up the standing wave by interference. Therefore, a backward propagating ionization front is generated, as seen in Fig.4. The density at the front exceeds the critical density. This feature is not obtained for a single pulse impinging on a dense target, since it undergoes immediate self-reflection and penetrates only in the "skin"surface layer (Macchi et al. 1999).

An example of "overdense" ionization front is obtained in the case of a CO_2 square pulse 15 cycles long impinging over a target with $n_e = 4n_c$. The $n_e(x,t)$ contour plot is shown in Fig.6. The ionized layers merge into a more homogeneous distribution and a "continuous" ionization front appears. The merging appears because the time- and space-modulated refractive index perturbs the reflected wave substantially, leading to broadening of interference maxima. The velocity of the front in Fig.6 is near to, or even exceeds at some times that of light. This is clearly not a physical "moving mirror" with a velocity greater than c, but a reflective surface which is created apparently with such velocity due to a space-time phase effect.

ACKNOWLEDGMENTS

We acknowledge the scientific contributions of D. Bauer and L. Plaja as well as their suggestions. Discussions with G. La Rocca, R. Colombelli, L. Roso, and V. Malyshev are also greatly acknowledged. This work has been supported by the European Commission through the TMR networks SILASI, contract No. ERBFMRX-CT96-0043, and GAUSEX, contract. No. ERBFMRX-CT96-0080. E.C.J. also acknowledges support from the Junta de Castilla y León (under grant SA56/99).

REFERENCES

BAUER, D. 1997 Phys. Rev. A **55**, 2180.

BAUER, D. & MULSER, P. 1999 Phys. Rev. A **59**, 569.

BRUNEL, F. 1990 J. Opt. Soc. Am. B **7**, 521.

BURSTEIN, E. & WEISBUCH, C., eds. 1993 *Confined Electrons and Photons. New Physics and Applications* (NATO ASI Series B: Physics, vol.340, Plenum Press, New York, 1993).

CONEJERO JARQUE, E., CORNOLTI, F. & MACCHI, A. 2000 J. Phys. B: At. Mol. and Opt. Phys. **33**, 1.

CORNOLTI, F., MACCHI, A. & CONEJERO JARQUE, E. 1998 in *Superstrong Fields in Plasmas*, Proceedings of the First International Conference (Varenna, Italy, 1997), edited by M. Lontano *et al.*, AIP Conf. Proc. No. **426** (AIP, New York, 1998), p.55.

GIULIETTI, D., GIZZI, L.A., GIULIETTI, A., MACCHI, A., TEYCHENNE, D., CHESSA, P., ROUSSE, A., CHERIAUX, G., CHAMBARET, J.P. & DARPENTIGNY, G. 1997 Phys. Rev. Lett. **79**, 3194.

MACCHI, A., CONEJERO JARQUE, E., BAUER, D., CORNOLTI, F. & PLAJA, L. 1999 Phys. Rev. E **59**, R36.

MULSER, P., CORNOLTI, F. & BAUER, D. 1998 Phys. of Plasmas **5**, 4466.

RAE, S. C. & BURNETT, K. 1992 Phys. Rev. A **46**, 1084.

SKOLNICK, M. S., FISHER, T. A. & WHITTAKER D. M. 1998 Semicond. Sci. Technol. **13**, 645.

TEYCHENNÉ, D., GIULIETTI, D., GIULIETTI, A. & GIZZI, L. A. 1998 Phys. Rev. **E58**, R1245.

WILKS, S. C., DAWSON, J. M. & MORI, W. B. 1988 Phys. Rev. Lett. **61**, 337.

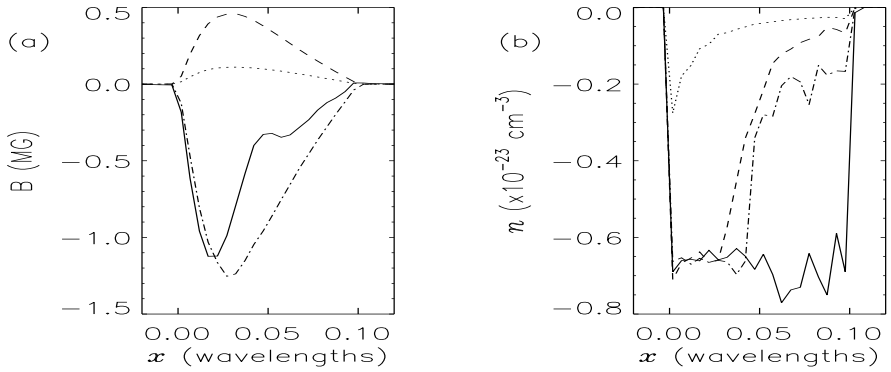

FIG. 1. Spatial distribution of magnetic field (left) and electron charge density (right) five cycles after the end of the pulse, for "$\sin^2$" pulses of 0.1 a.u. (dotted line), 1 a.u. (dashed line), 10 a.u. (solid line) maximum amplitude and a "square" pulse of 1 a.u. amplitude (dashed-dotted line). All the pulses are 5 cycles long. The electric field atomic unit is $E_{au} = 5.1 \times 10^9$ V cm^{-1} (corresponding to $I = 3.5 \times 10^{16}$ W cm^{-2}).

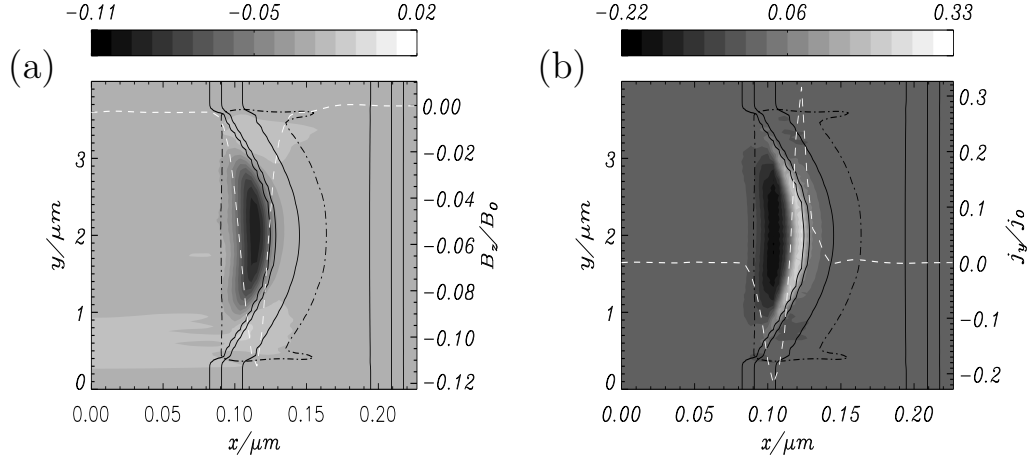

FIG. 2. Grayscale contours of the magnetic field B_z (a) and the current density j_y (b) five laser cycles after the laser pulse end, for a 2D2V Boltzmann simulation. The dashed line in (a) and (b) give B_z/B_o and j_y/j_o, respectively, along $x = 2\mu m$. The parameters $B_o = 27.7$ MG, $j_o = 2.2 \times 10^{22}$ c.g.s. units. The solid lines give neutral density contours. The dashed-dotted lines mark the critical density surface. Simulation parameters $I = 10^{16}$W cm^{-2}, $\lambda = 0.25\mu$m, $n_e/n_c = 12.5$.

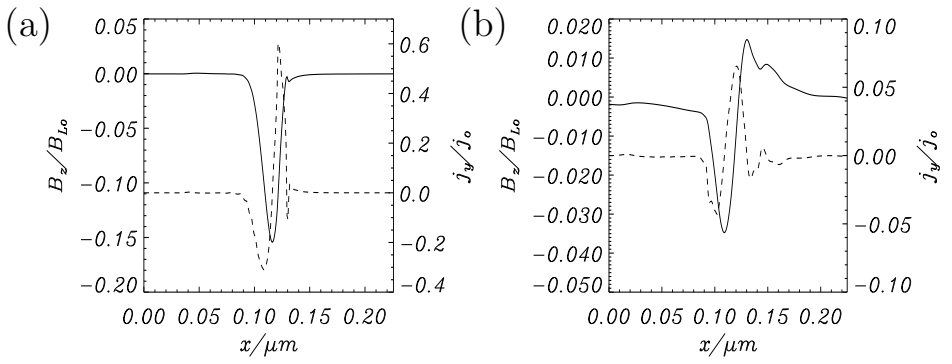

FIG. 3. Profiles of the steady magnetic field B_z (solid) and the current j_y (dashed) in 1D Boltzmann simulations. The parameters common to (a) and (b) are $\lambda = 0.25\,\mu$m and $n_e/n_c = 12.5$. In the case (a) the atomic parameters are those of an hydrogenlike atom with $Z = 1$, and $I = 10^{16}$W cm^{-2}, $B_o = 27.7$ MG, $j_o = 2.2{\times}10^{22}$ c.g.s. units. In the case (b) $Z = 2$ and laser parameters are scaled accordingly to $\mathbf{x} \to Z\mathbf{x}$, $t \to Z^2 t$, $\omega \to Z^{-2}\omega$, $\mathbf{E} \to Z^{-3}\mathbf{E}$; $I = 6.4 \times 10^{17}$W cm^{-2}, $B_o = 50.6$ MG, $j_o = 7 \times 10^{22}$ c.g.s. units.

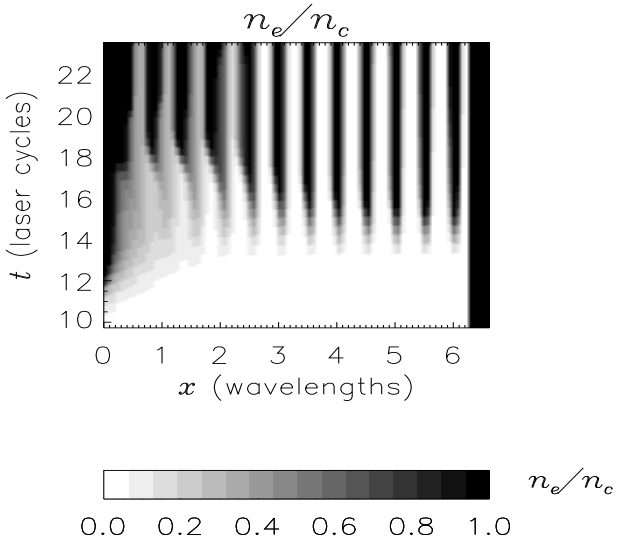

FIG. 4. Grayscale contourplot of free electron density $n_e(x,t)$ for a "solid" hydrogen target with a reflecting "metal" layer on the rear face (thick solid line). The pulse parameters are $I = 1.8 \times 10^{14}$ W cm^{-2}, $\lambda = 0.8\,\mu$m, $\Delta t_L = 30(2\pi/\omega_L) \simeq 80$ fs ("sin^2" envelope). The target parameters are $L = 2\pi\lambda$, $n_o = 10n_c = 1.1 \times 10^{22}$ cm^{-3}.

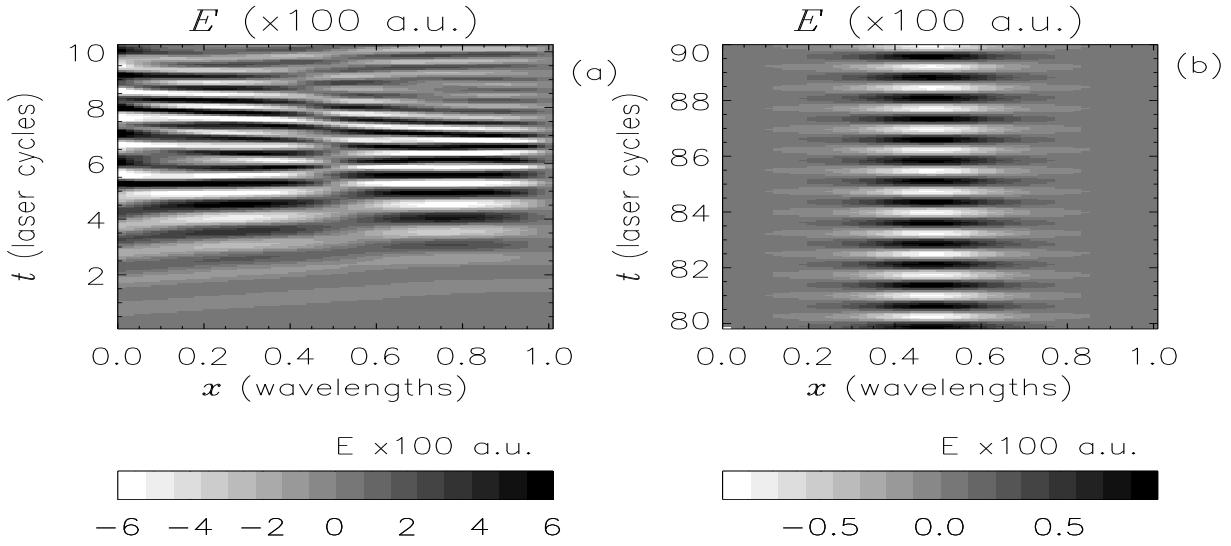

FIG. 5. Evolution of the electric field inside the plasma slab during the interaction with the incident pulse (a) and 80 cycles later (b). The pulse parameters are $I = 1.8 \times 10^{14}$ W cm^{-2}, $\lambda = 10.6\,\mu m$, $\Delta t_L = 15(2\pi/\omega_L) \simeq 530$ fs ("sin^2" envelope). The target parameters are $L = \lambda$, $n_o = 5n_c = 5 \times 10^{19}$ cm^{-3}.

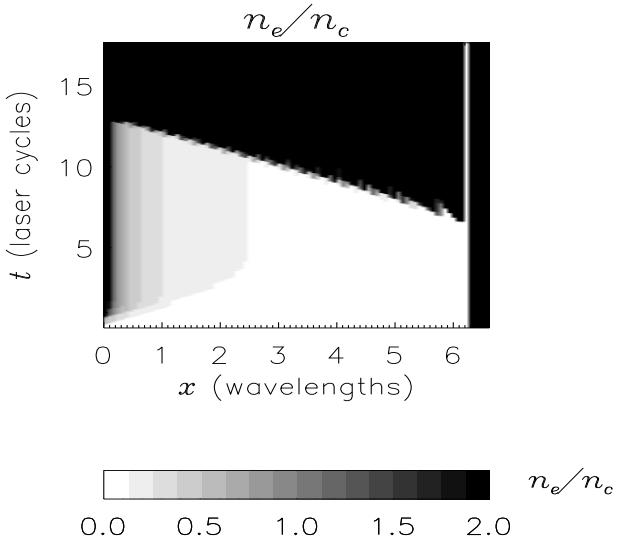

FIG. 6. Grayscale contourplot of $n_e(x,t)$ for a hydrogen "gaseous" target with a reflecting "metal" layer on the right boundary. The pulse has square envelope and parameters $I = 1.8 \times 10^{14}$ W cm^{-2}, $\lambda = 10.6\,\mu m$, $\Delta t_L = 15(2\pi/\omega_L) \simeq 530$ fs Target parameters are $L = 2\pi\lambda$, $n_e = 4n_c = 4 \times 10^{19}$ cm^{-3}.